Nanoscale

PAPER

View Article Online
View Journal | View Issue

Cite this: *Nanoscale*, 2017, **9**, 10335

Analogous self-assembly and crystallization: a chloride-directed orientated self-assembly of Cu nanoclusters and subsequent growth of $Cu_{2-x}S$ nanocrystals†

Jiale Liu,[a] Ye Tian,[a] Zhennan Wu,[a] Lin Ai,[a] Yi Liu,[a] Jianli Cui,*[b] Weili Yu,[c] Hao Zhang*[a] and Bai Yang[a]

Received 4th May 2017,
Accepted 15th June 2017

DOI: 10.1039/c7nr03161k

rsc.li/nanoscale

Self-assembly and crystallization are two common methods to control the morphologies of nanomaterials, which have many similarities. In this work, chloride is used to direct the self-assembly process of Cu nanoclusters and the subsequent growth of $Cu_{2-x}S$ nanocrystals. Meaningfully, chloride both promotes the transformation of Cu nanocluster self-assembled architectures from one-dimensional (1D) to 2D, and facilitates the transformation of $Cu_{2-x}S$ nanocrystals from nanorods to nanosheets. Such an influence is attributed to the selective adsorption of chloride ions on the specific facets of nanoclusters and nanocrystals, which alters the inter-nanocluster weak interactions during self-assembly and suppresses the activity of $Cu_{2-x}S$ facets during nanocrystal growth. The current results indicate that the method used to direct the morphologies of nanocrystals is extendable to control the tendency of nanocluster self-assembly.

1. Introduction

The past two decades have witnessed the controllable synthesis of inorganic nanomaterials by tailoring their morphologies, which significantly determine the electronic structures and the subsequent functionalities of the materials.[1–10] Controllable crystallization and self-assembly are two common approaches to adjust the morphologies of inorganic nanomaterials.[3–18] Crystallization is the process in which atoms arrange in highly ordered microscopic structures on the basis of strong interactions, such as metallic bonds, covalent bonds, and so forth.[19] As for self-assembly, building blocks including nanometer-sized clusters or particles, and various weak interactions, such as electrostatic, dipolar, and van der Waals (vdW) interactions, are employed to direct the self-assembly process.[11–18,20–22] In this scenario, both crystallization and self-assembly are the methods that convert the building blocks into ordered structures. The difference between crystallization and self-assembly is the size of building blocks and the intensity of driving forces.

Controlled synthesis of nanocrystals with desired morphologies has been intensively investigated.[3–10] Many approaches have been employed to tailor the size and morphologies of nanocrystals on the basis of thermodynamic and kinetic control, such as the reaction temperature, precursor concentration, and in particular the selective suppression of the growth along specific crystalline facets using capping ligands and/or additives.[23–27] Clear comprehension of the growth mechanism of nanocrystals makes it easy to engineer the morphologies from spherical particles to one-dimensional (1D) nanorods and 2D nanosheets.[28–30] However, the controllable self-assembly of nanoclusters is more difficult, because of the complex influencing factors and therefore the unclear self-assembly process.[31–33] In addition, the driving forces are so weak that the self-assembly process is greatly influenced by environmental factors, such as the interfacial effect of solvents, thermal disturbance, and so forth.[31–35] To direct the self-assembly, the nanoclusters should be initially endowed with appropriate surface functionalities to introduce the driving force.[36–39] Meanwhile, the entropy effect must be considered in the self-assembly process, such as that arising from temperature, solvent polarity and stirring rate, because it usually offsets the interactions between the nanoclusters and

[a]State Key Laboratory of Supramolecular Structure and Materials, College of Chemistry, Jilin University, Changchun 130012, P. R. China. E-mail: hao_zhang@jlu.edu.cn
[b]Department of Hand & Foot Surgery, The First Hospital of Jilin University, Changchun 130021, P. R. China. E-mail: tsuijianli@126.com
[c]The China-US Joint Laboratory, Changchun Institute of Optics, Fine Mechanics and Physics, Chinese Academy of Science, Changchun, 130033, P. R. China

†Electronic supplementary information (ESI) available: Additional experimental information, XPS, XRD and UV-vis absorption spectra, MALDI-TOF MS, TEM and AFM images of Cu nanocluster self-assembled architectures and $Cu_{2-x}S$ nanocrystals. See DOI: 10.1039/c7nr03161k

increases the difficulty in self-assembly.[31–35] This means that despite the fact that the manipulation of atom arrangement has been well established, the arrangement of nanoclusters into regular structures is still challenging. It is considered that establishing the relationship between crystallization and self-assembly by exploring their similarity will promote the development of self-assembly techniques.

It is known that halides play an important role in directing the growth of nanocrystals.[40–42] They usually adsorb on specific crystalline facets, and suppress or facilitate the crystal growth along these facets, thus resulting in different morphologies.[26,43] For example, Kim *et al.* synthesized octapod-shaped CdSe/CdS nanocrystals and observed a shape evolution from octapods to tetrapods by dosing $CdCl_2$ together with CdO as cadmium sources.[44] Meyns *et al.* studied the shape evolution of CdSe nanorods to hexagonal pyramids under the influence of halogenated additives in the form of organic chlorine, bromine and iodine compounds.[45] Lohse *et al.* indicated the possible roles of halides in the synthesis of anisotropic noble metal nanocrystals.[46] However, the role of halides in the self-assembly of nanoclusters is scarcely mentioned. In this context, establishing the similarity between crystallization and self-assembly is capable of extending the well-studied halide-directed nanocrystal growth to perform the orientated self-assembly of nanoclusters.

In this paper, the similarity between the chloride-directed orientated self-assembly of Cu nanoclusters and the subsequent growth of $Cu_{2-x}S$ nanocrystals is studied. Chloride promotes both the transformation of Cu nanocluster self-assembled architectures from nanowires to nanosheets and the growth of $Cu_{2-x}S$ nanocrystals from nanorods to nanosheets. The morphology transfer from 1D to 2D is attributed to the selective adsorption of chloride ions (Cl^-) on nanocluster and nanocrystal surfaces. The Cl^- suppression facilitates the self-assembly of Cu nanoclusters and the growth of $Cu_{2-x}S$ nanocrystals with 2D tendency.

2. Experimental

2.1. Materials

1-Dodecanethiol (DT, 98%) was purchased from Aladdin Chemistry Co. Ltd. Dibenzyl ether (BE, 98%) was purchased from Aldrich. Copper(II) 2,4-pentanedionate ($CuAc_2$, 98%) was purchased from Aldrich. Liquid paraffin (LP, CP) was purchased from Sinopharm Chemical Reagent Co. Ltd. Copper chloride ($CuCl_2{\cdot}2H_2O$, 99%, A. R.), copper bromide ($CuBr_2$, 99%, AR), copper iodide (CuI, 98%, CP), acetone, and chloroform were all commercially available products and used as received without further purification.

2.2. Preparation of Cu nanocluster self-assembly architectures

Cu nanoclusters were prepared and assembled into different architectures by stirring a mixture of 6 mL LP, 6 mL BE, 2 mL DT, $CuCl_2{\cdot}2H_2O$ and $CuAc_2$ with a specific molar ratio at room temperature. Then the mixture was heated to 120 °C for 10 min. After fixing the Cu^{2+} concentration at 0.5 mmol and adjusting the $CuCl_2$-to-$CuAc_2$ molar feed ratio from 0/10, 0.05/9.5, 1/9, 2/8, 3/7, 5/5 and 7/3 to 10/0, the as-prepared assemblies change from self-assembled nanowires (SANWs), self-assembled nanoribbons (SANRs) to self-assembled nanosheets (SASs).

2.3. Preparation of Cu_2S nanorods from Cu SANWs

The as-prepared Cu SANW solution was heated to 220 °C within 10 min. Then, the solution was kept at 220 °C for 120 min and cooled down slowly.

2.4. Preparation of Cu_2S nanodisks from Cu SANRs

The as-prepared Cu SANR solution was heated to 220 °C within 10 min. Then, the solution was kept at 220 °C for 120 min.

2.5. Preparation of $Cu_{1.8}S$ nanosheets from Cu SASs

The as-prepared Cu SAS solution was heated to 220 °C within 10 min. Then, the solution was kept at 220 °C for 120 min.

2.6. Purification

At room temperature, 1 mL solution of the products was washed and precipitated by adding 1 mL chloroform and 2 mL acetone. After that, the products were separated by centrifugation at 6000 rpm for 5 min. The purification process was repeated twice. Finally, the precipitates were collected and dispersed in 1 mL chloroform.

2.7. Characterization

Transmission electron microscopy (TEM) images were obtained by using a JEM-2100F electron microscope at an acceleration voltage of 200 kV. An energy-dispersive X-ray spectroscopy (EDX) detector coupled with TEM was used for elemental analysis. Atomic force microscopy (AFM) tapping mode measurements were performed with a Nanoscope IIIa scanning probe microscope (Digital Instruments) using a rotated tapping mode etched silicon probe tip. X-ray diffraction (XRD) investigations were carried out on a PANalytical B.V.-Empyrean Diffractometer using Cu Kα radiation (λ = 1.5418 Å). Matrix-assisted laser desorption/ionization time of flight (MALDI-TOF) mass spectra were recorded on a Bruker Autoflex speed TOF/TOF, where THF and *trans*-2-[3-(4-*tert*-butylphenyl)-2-methyl-2-propenylidene]malononitrile were used as the solvent and matrix to dissolve the samples. UV-vis absorption spectra were obtained using a Shimadzu 3600 UV-VIS-NIR spectrophotometer. X-ray photoelectron spectroscopy (XPS) was investigated with a VG ESCALAB MKII spectrometer.

3. Results and discussion

3.1. Chloride-directed orientated self-assembly of Cu nanoclusters

The Cu nanoclusters employed to fabricate self-assembled architectures are prepared in mixtures of LP and BE using

$CuCl_2$ and $CuAc_2$ as the Cu sources and DT as the capping ligand at room temperature. Then the Cu nanocluster solution is heated to 120 °C. By altering the $CuCl_2$-to-$CuAc_2$ molar feed ratio from 0/10, 0.5/9.5, 1/9, 2/8, 3/7, 5/5 and 7/3 to 10/0, Cu nanocluster self-assembled architectures with different morphologies are fabricated. In general, with the increase of $CuCl_2$ ratio, the self-assembled architectures convert from 1D SANWs to 2D SANRs and SASs (Fig. S1†). Fig. 1 shows the TEM images of SANWs, SANRs, and SASs, which are prepared with $CuCl_2$-to-$CuAc_2$ ratios of 0/10, 2/8, and 10/0. The high magnification TEM images show that the SANWs, SANRs, and SASs are composed of small clusters with diameters below 2 nm (Fig. S2†). By combining the TEM observation, MALDI-TOF mass spectra, UV-vis absorption spectra, and XPS measurements, it is concluded that the composition of the nanoclusters in SANWs, SANRs, and SASs is the same, which is $Cu(0)_4Cu(I)_{10}DT_{10}$ (Fig. S2–S5†).[47] To confirm the existence of chloride, the SANWs, SANRs, and SASs are purified and characterized by XPS (Fig. S5†), which shows the increase of chloride from SANWs to SANRs and SASs. This tendency is further proved by EDX analysis (Fig. S6†). There is no chloride in the SANWs, while the Cu-to-Cl atomic ratio is 6.89 and 3.55 in SANRs and SASs, respectively. This means that there are about two and four Cl^- ions adsorbed on the Cu nanoclusters in SANRs and SASs. The aforementioned results imply the influence of chloride on the morphologies of Cu nanocluster self-assembled architectures.

The SANWs, SANRs and SASs are further characterized by XRD. Both the small-angle and wide-angle XRD patterns indicate that the self-assembled architectures are composed of ordered and small building blocks (Fig. S7†). By comparing with the small-angle and wide-angle XRD patterns of $CuAc_2$, the influence of the local structures of $CuAc_2$ on self-assembled architectures is excluded (Fig. S8†). According to our previous studies,[31,32,47] the self-assembly of Cu nanoclusters is determined both by the dipolar attraction between Cu nanoclusters and the vdW attraction between the capping ligand DTs. The small-angle XRD patterns present the first order peak at 2.51° and 2.61° for SANWs and SASs, respectively. But the SANRs show two peaks at 2.54° and 2.64°. As for SANWs and SASs, the sole small-angle XRD peak means that there is only one dominant distance between the composed Cu nanoclusters, implying that the self-assembly of Cu nanoclusters is favored only along one direction.[31] By combining the TEM observation (Fig. 1), the self-assembly direction of SANWs should be along the "axis", while it is along the "plane" direction of the SASs. For the SANRs, the two small-angle XRD peaks indicate that the self-assembly involves two directions,[31] thus generating ribbon structures. In addition, with the increase of chloride, the tendency of self-assembly along the "axial" direction decreases and the self-assembly along the "plane" direction increases. So, we propose that the adsorption of Cl^- is mainly in the axial direction, namely along the direction of the dipole.[31] This leads to a redistribution of DT alkyl chains by bending to the "plane" direction. The favorable distribution of DT in the "plane" direction in return suppresses the nanocluster assembly along the "axial" direction by decreasing the dipolar attraction, promoting the self-assembly with 2D tendency.[31,32] This consideration is proved by the small-angle XRD data that the inter-nanocluster distance along the "axial" direction decreases and that along the "plane" direction increases, because the DT alkyl chains along the "axis" bend toward the "plane" (Fig. S7a†). In the absence of chloride, the strong dipolar attraction between the neighboring Cu nanoclusters drives the self-assembly along the "axial" direction, producing 1D SANWs. With the addition of chloride, the bent DT alkyl chains toward the "plane" direction decrease the dipolar attraction but increase the vdW attraction along the "plane" direction through the overlapping of DT alkyl chains. Besides, the adsorbed Cl^- also suppresses the self-assembly along the "axial" direction, because of static repulsion. As a result, the strong dipolar attraction drives the self-assembly of Cu nanoclusters into 1D SANWs along the "axial" direction in the absence of chloride. With lower Cl^- adsorption, the nanocluster self-assembly along the "axial" direction is suppressed and the self-assembly along the "plane" direction is favored, thus producing SANRs. With higher Cl^- adsorption, the self-assembly along the "plane" direction is dominant, which produces SASs.

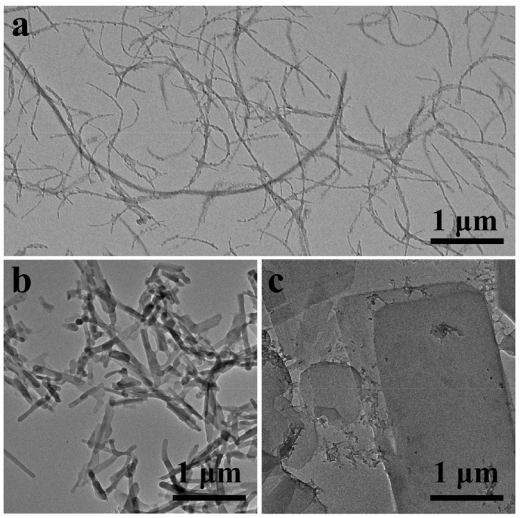

Fig. 1 TEM images of the self-assembled architectures of Cu nanoclusters that are prepared with $CuCl_2$-to-$CuAc_2$ molar feed ratios of 0/10 (a), 2/8 (b) and 10/0 (c).

3.2. Transformation of SANWs to $Cu_{2-x}S$ nanorods

On heating the Cu nanocluster SANWs at 220 °C for 120 min, $Cu_{2-x}S$ nanorods are prepared. The transformation process from Cu SANWs to $Cu_{2-x}S$ nanorods is monitored by TEM (Fig. 2). Note that the Cu SANWs are prepared at 120 °C using $CuAc_2$ as the Cu source in the absence of chloride. When the SANW solution is heated to 160 °C, the morphology of 1D SANWs remains unchanged. The size of the clusters remains at 1.9 ± 0.3 nm, which is the same as that of Cu nanoclusters at 120 °C. Further increasing the temperature to 210 °C and

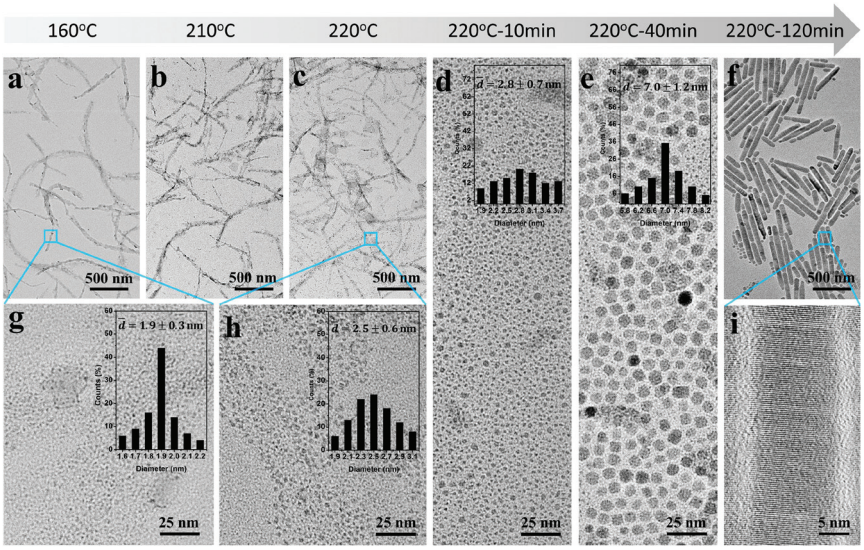

Fig. 2 The process tracking TEM images of Cu_2S nanorods at 160 °C (a), 210 °C (b), 220 °C (c), 220 °C for 10 min (d), 220 °C for 40 min (e) and 220 °C for 120 min (f). (g) and (h) are the high magnification TEM images of (a) and (c). (i) is the HRTEM image of (f). The inset pictures in (d), (e), (g) and (h) are their corresponding size distributions.

finally to 220 °C, the morphology of nanowires is destroyed and the small clusters start fusing into larger ones. The size of the clusters reaches 2.5 ± 0.6 nm at 220 °C, which means the fusion of two or three clusters into one at this time. Small-angle XRD data show the shift of the first order peak from 2.51° to 2.48° and 2.45° at 160 °C, 210 °C and 220 °C (Fig. S9a†). The calculated inter-nanocluster distances are 3.52, 3.56 and 3.61 nm.[47] The increase of inter-nanocluster distances results from the size increment of the clusters. No obvious diffraction peaks are observed in the wide-angle XRD region, indicating that the Cu SANWs do not transform into highly crystalline $Cu_{2-x}S$ before 220 °C (Fig. S9b†).[48] These results reveal that the SANWs are stable at 160 °C, but the DT will decompose and release S to support the growth of $Cu_{2-x}S$ over 200 °C.[49] As a result, the small Cu nanoclusters gradually fuse into bigger ones and react with the released S.

On prolonging the duration at high temperature, the decomposition of DTs is greatly facilitated, which accelerates the growth of $Cu_{2-x}S$ nanocrystals by supplying more S.[49] This is like the nucleation stage of $Cu_{2-x}S$ nanocrystals according to the classic growth process of colloidal nanocrystals. First, the Cu nanoclusters fuse and react with S into 2.5 ± 0.6 nm $Cu_{2-x}S$ nuclei at 220 °C. Then the $Cu_{2-x}S$ nuclei grow into 2.8 ± 0.7 nm quasi-spherical particles after 10 min at 220 °C. After 40 min, these $Cu_{2-x}S$ particles grow up to 7.0 ± 1.2 nm particles. Finally, these small $Cu_{2-x}S$ nanoparticles transform into $Cu_{2-x}S$ nanorods as maintained at 220 °C for 120 min (Fig. 2). The nanorods are about 72.5 ± 29.1 nm in length and 9.9 ± 1.1 nm in width. Fig. S10† shows the UV-vis absorption spectra during the growth of $Cu_{2-x}S$ nanorods. In comparison with the quasi-spherical particles, the $Cu_{2-x}S$ nanorods show enhanced absorption around 500 nm, which consists with the previous report.[28] The small-angle XRD peaks, which correspond to the inter-nanocluster distance of Cu SANWs, start to disappear, and the wide-angle XRD peaks, which correspond to the lattice spacing, start to appear after heating at 220 °C for 10 min (Fig. S9†). This implies the transformation of Cu nanoclusters to $Cu_{2-x}S$ nanocrystals.[50] In addition, the EDX result reveals the Cu-to-S molar ratio of $Cu_{2-x}S$ nanorods as 2 : 1, showing the composition of Cu_2S (Fig. S11†). The wide-angle XRD patterns also indicate that the diffraction peaks of the nanorods consist with hexagonal Cu_2S (chalcocite, JCPDS no. 26-1116). The high-resolution TEM (HRTEM) images show that the (002) crystal facets are dominant both for the Cu_2S nanoparticles and nanorods (Fig. S12†). According to the oriented attachment mechanism of nanorod growth,[51] the formation of Cu_2S nanorods is considered through the attachment and fusion of small Cu_2S nanoparticles along the [002] direction, which also corresponds to the "axial" direction of Cu SANWs.

3.3. Transformation of SANRs to $Cu_{2-x}S$ nanodisks

The morphology of $Cu_{2-x}S$ nanocrystals greatly depends on the morphology of the original Cu nanocluster self-assembled architectures. On heating the Cu SANRs at 220 °C for 120 min, the final products obtained are $Cu_{2-x}S$ nanodisks (Fig. 3). Similar to the growth of $Cu_{2-x}S$ nanorods, the formation of $Cu_{2-x}S$ nanodisks also starts with the fusion of Cu nanoclusters after continuously heating. The difference is the adsorption of Cl^- on the as-assembled Cu nanoclusters. In the presence of chloride, the fusion of Cu nanoclusters shows obvious anisotropy. It can be seen from the TEM images that after heating to 220 °C, there exist stripes in the intermediates, which are the fused nanoclusters (Fig. 3c and h†). These mean the presence of intermediates between the nanoclusters and nanocrystals or the nanocrystals with poor crystallinity during the formation of $Cu_{2-x}S$ nanodisks. In the wide-angle XRD

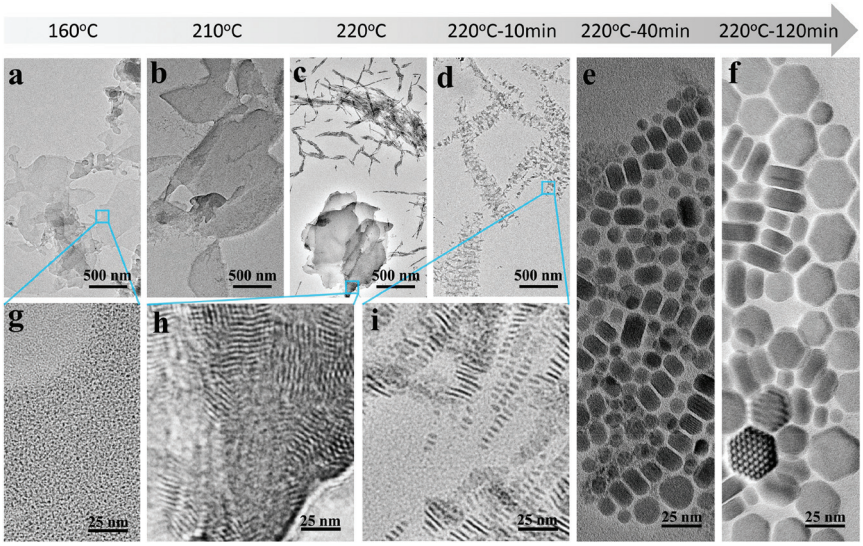

Fig. 3 The process tracking TEM images of Cu_2S nanodisks at 160 °C (a), 210 °C (b), 220 °C (c), 220 °C for 10 min (d), 220 °C for 40 min (e) and 220 °C for 120 min (f). (g), (h) and (i) are the high magnification TEM images of (a), (c) and (d).

pattern, a weak peak at about 46° is found when the temperature rises to 220 °C (Fig. S13b†), which corresponds to the (110) facets of hexagonal $Cu_{2-x}S$ nanocrystals.[52–54] This peak significantly enhances after heating at 220 °C for 10 min. No other $Cu_{2-x}S$ diffraction peaks are observed, implying the tiny structure of the $Cu_{2-x}S$. After heating at 220 °C for 120 min, the $Cu_{2-x}S$ further evolves into nanodisks (Fig. 3f). The EDX result of $Cu_{2-x}S$ nanodisks reveals the Cu-to-S molar ratio of 2 : 1, presenting the composition of Cu_2S (Fig. S14†). The nanodisks are determined as hexagonal Cu_2S by XRD (chalcocite, JCPDS no. 26-1116). HRTEM images indicate that the top and bottom surfaces of the nanodisks are dominant by the interplanar spacing of 0.199 nm, while the sides are dominant by the interplanar spacing of 0.337 nm (Fig. S15†). This result implies that the Cl^- may adsorb on the (002) facets, which suppresses the growth and fusion of small Cu_2S along the [002] direction, thus producing Cu_2S nanodisks.

Fig. S13a† shows the small-angle XRD patterns as the transformation from Cu SANRs to Cu_2S nanodisks occurs. The gradual decrease of the small-angle XRD peaks means the destruction of the Cu nanocluster self-assembled architectures. When Cu SANRs are heated to 160 °C, 210 °C and 220 °C, the first order peak shifts from 2.49° to 2.47° and 2.44°, which is similar to the evolution of Cu SANWs. This reveals the increase of the distance between nanoclusters during the fusion. The difference is the appearance of a strong diffraction peak at 1.76° after heating at 220 °C for 10 min, corresponding to the distance of 5.02 nm, which is attributed to the closely packed tiny Cu_2S disks (Fig. 3d and i). After heating at 220 °C for 120 min, these tiny disks grow into nanodisks with 35.5 ± 4.9 nm width and 11.6 ± 0.7 nm thickness. The UV-vis absorption spectra are almost the same at 160 °C, 210 °C and 220 °C (Fig. S16†). The unchanged peaks below 400 nm mean the existence of Cu nanoclusters. After heating at 220 °C for 120 min, a strong absorption peak appears around 500 nm, showing the formation of thick Cu_2S nanodisks and consisting with the previous reports.[55,56] By analyzing the transformation process from Cu SANRs to Cu_2S nanodisks, it can be safely mentioned that the adsorbed Cl^- influences both Cu nanocluster self-assembly and their fusion into $Cu_{2-x}S$ nanocrystals. Cl^- is capable of suppressing the self-assembly and further fusion of nanoclusters along the Cl^--adsorbed direction.

3.4. Transformation of SASs to $Cu_{2-x}S$ nanosheets

As mentioned above, the Cu nanocluster SASs are prepared using $CuCl_2$ as the Cu source, which leads to the adsorption of more Cl^- on nanoclusters than SANRs. The transformation of Cu nanocluster self-assembly architectures to $Cu_{2-x}S$ nanosheets is similar to that of nanorods and nanodisks. With the increase of temperature, the nanoclusters show 2D fusion first (Fig. 4). Then the fused nanoclusters transform into tiny and thin nanosheets at 220 °C for 10 min. Finally, the small tiny nanosheets grow into larger ones with prolonged heating duration. The size of the final nanosheets is about 93.4 ± 24.8 nm in width and 4.4 nm in thickness (Fig. S17†). According to the discussions about the chloride-directed growth of Cu_2S nanodisks, the formation of thinner $Cu_{2-x}S$ nanosheets results from the adsorption of more Cl^- on the top and bottom surfaces of $Cu_{2-x}S$ nanosheets, thus facilitating the growth with a 2D feature. The first order peak in small-angle XRD patterns shifts from 2.61° to 2.51° and 2.51° at 160 °C, 210 °C and 220 °C, which shows the change of the inter-nanocluster distance (Fig. S18†). The small-angle XRD peak at 1.99° is still strong after heating at 220 °C for 10 min, which is caused by the distance between the packed tiny nanosheets.[31] The calculated distance of 4.44 nm is shorter than that of the intermediates for prepar-

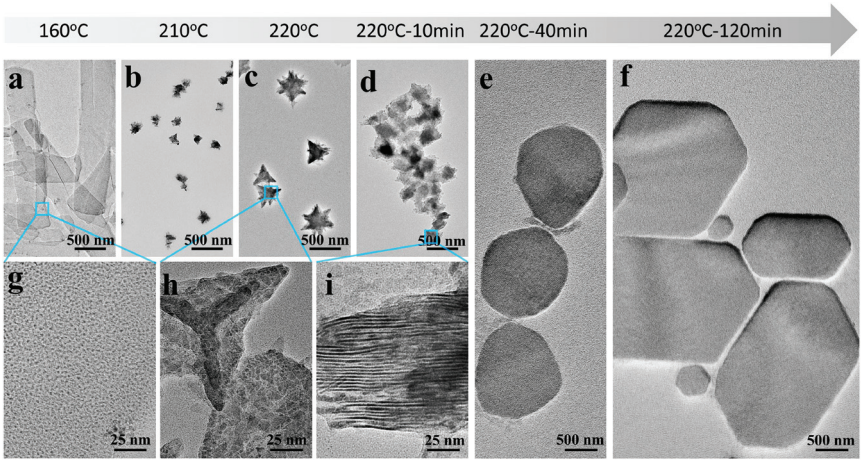

Fig. 4 The process tracking TEM images of $Cu_{1.8}S$ nanosheets at 160 °C (a), 210 °C (b), 220 °C (c), 220 °C for 10 min (d), 220 °C for 40 min (e) and 220 °C for 120 min (f). (g), (h) and (i) are the high magnification TEM images of (a), (c) and (d).

ing $Cu_{2-x}S$ nanodisks, which is 5.02 nm. This means that the intermediates of nanosheets are thinner than that of nanodisks, representing the role of adsorbed Cl^- in directing the facet-selective growth. The wide-angle XRD data also show the transformation from Cu nanoclusters to $Cu_{2-x}S$ nanocrystals at 220 °C, because of the appearance of the peak at about 46°.[52–54] This peak becomes obvious after heating at 220 °C for 10 min. Hexagonal Cu_2S nanosheets are found after 40 min (chalcocite, JCPDS no. 26-1116), but transform into hexagonal $Cu_{1.8}S$ nanosheets after 120 min (digenite, JCPDS no. 23-0962). The $Cu_{1.8}S$ nanosheets show enhanced absorption compared to Cu_2S nanosheets (Fig. S19†). Note that the single diffraction peak at 46° corresponds to the hexagonal (110) facets of ultrathin $Cu_{2-x}S$ nanosheets, while the (102) and (103) facets are not found.[52] Since the (002) facets are vertical to the (110) facets, we propose that the growth along the (002) facets is strongly suppressed. By HRTEM observation, it can be concluded that the top and bottom surfaces of $Cu_{2-x}S$ nanosheets are (002) facet-terminated (Fig. S20†). The adsorption of Cl^- on the (002) facets suppresses the growth and thereby leads to the 2D growth of nanosheets. So, with the increase of chloride, the thickness of $Cu_{2-x}S$ nanocrystals becomes thinner (Fig. 5).

$CuBr_2$ and CuI are also employed as Cu sources to direct the self-assembly of Cu nanoclusters and the subsequent growth of $Cu_{2-x}S$ nanocrystals. According to the TEM observation (Fig. S22†), the roles of Br^- and I^- are different from Cl^-. When the Cu source is $CuBr_2$, the as-assembled Cu nanoclusters appear as a mixture of sheets and star-like balls. In the following growth of $Cu_{2-x}S$, the products are ultra-long nanorods. When the Cu source is CuI, the morphology of the Cu nanocluster self-assembled architecture is irregular. The following growth of $Cu_{2-x}S$ also produces irregular nanocrystals. These results mean that chloride is specific for directing the morphology evolution of Cu nanocluster self-assembled architectures and $Cu_{2-x}S$ nanocrystals.

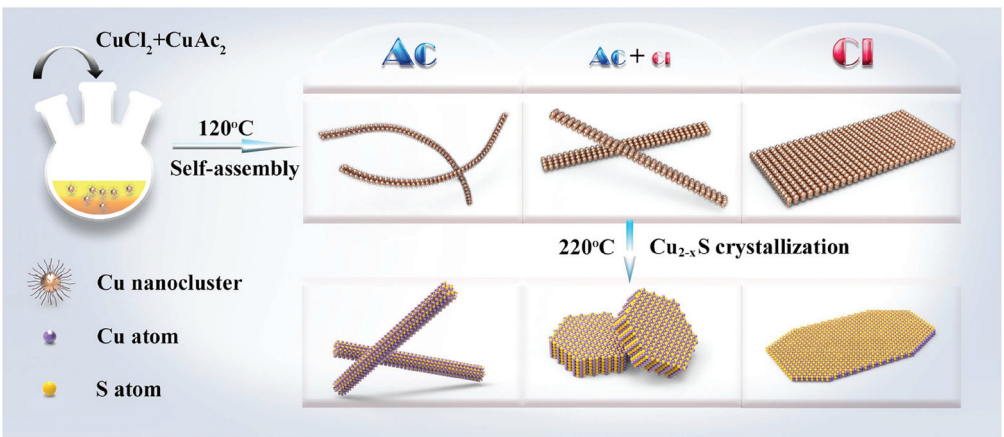

Fig. 5 Schematic illustration of the influence of chloride on the morphologies of Cu nanocluster self-assembled architectures and $Cu_{2-x}S$ nanocrystals.

To monitor the chloride-directed morphology and spectral evolution of $Cu_{2-x}S$ nanocrystals, the $CuCl_2$-to-$CuAc_2$ molar feed ratio is adjusted from 0/10 to 0.5/9.5, 1/9, 2/8, 3/7, 5/5, 7/3 to 10/0 (Fig. 6a–h and S21†). The size and diameter–thickness ratios are calculated and indicated in Table S1† and Fig. 6i, where the diameter and thickness are obtained from TEM observation except that the thickness of $Cu_{1.8}S$ nanosheets is measured by atomic force microscopy (Fig. S17†). The diameter–thickness ratio increases with the increase of chloride. According to the wide-angle XRD data (Fig. 7), the (102) and (103) peaks of $Cu_{2-x}S$ fall off with the increase of chloride. On the one hand, the variation of the intensity of the (102) and (103) peaks indicates the change in the thickness of $Cu_{2-x}S$.[57] On the other hand, the decrease of the XRD peaks at 37° and 46° and the increase at 23° and 32° reveal the transformation from hexagonal Cu_2S to hexagonal $Cu_{1.8}S$,[58] which is the same as the transformation from small Cu_2S nanosheets to ultrathin $Cu_{1.8}S$ nanosheets after heating at 220 °C for 120 min. The transformation from Cu_2S to $Cu_{1.8}S$ is analyzed by comparing their atomic arrangement (Fig. S23 and S24†).[59] In comparison with $Cu_{1.8}S$, the unit cell of Cu_2S is much simpler. The unit cell of $Cu_{1.8}S$ contains twenty seven Cu atoms and fifteen S atoms. The missing process of three Cu atoms is shown in Fig. S24.† Accordingly, the unit cells of Cu_2S and $Cu_{1.8}S$ are packed into an integrated period to reveal the change in the atom arrangement. In this context, the Cu and S atoms in Cu_2S are regular in the same plane. The structure and composition of different planes are the same with only an atomic dislocation configuration. The atom arrangements along the *c* axis are shown in Fig. S23b and S24b.† It is found that they are the same along the *c* axis. However, great changes are found along the *b* axis of $Cu_{1.8}S$. The plane structure of Cu and S is destroyed, though the same plane atoms are found in the packed structure of $Cu_{1.8}S$. Only half of the Cu atoms in two planes are pushed out regularly. The calculated result indicates that there are 10% Cu atoms missing in the pushing process, consisting with the composition change from Cu_2S to $Cu_{1.8}S$. These results show that the transformation from Cu_2S to $Cu_{1.8}S$ lowers the regularity of the Cu atom arrangement. In addition, the process of Cu missing also relates to the thickness of nanocrystals, since thinner structures are beneficial to push Cu away. This also explains the transformation from Cu_2S to $Cu_{1.8}S$ with the increase of chloride. After transformation, the bond length also changes obviously. The bond lengths of Cu_2S are 2.245 Å in plane and 3.335 Å out of plane. For $Cu_{1.8}S$, the bond lengths reduce to 2.269, 2.292, 2.407, 2.779 and 2.888 Å. The shortening of the average bond lengths increases the thermodynamic stability of nanocrystals.

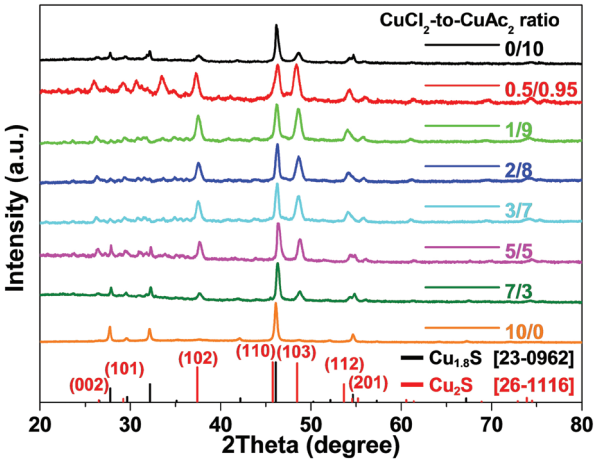

Fig. 7 Wide-angle XRD patterns of $Cu_{2-x}S$ nanocrystals with different $CuCl_2$-to-$CuAc_2$ molar feed ratios.

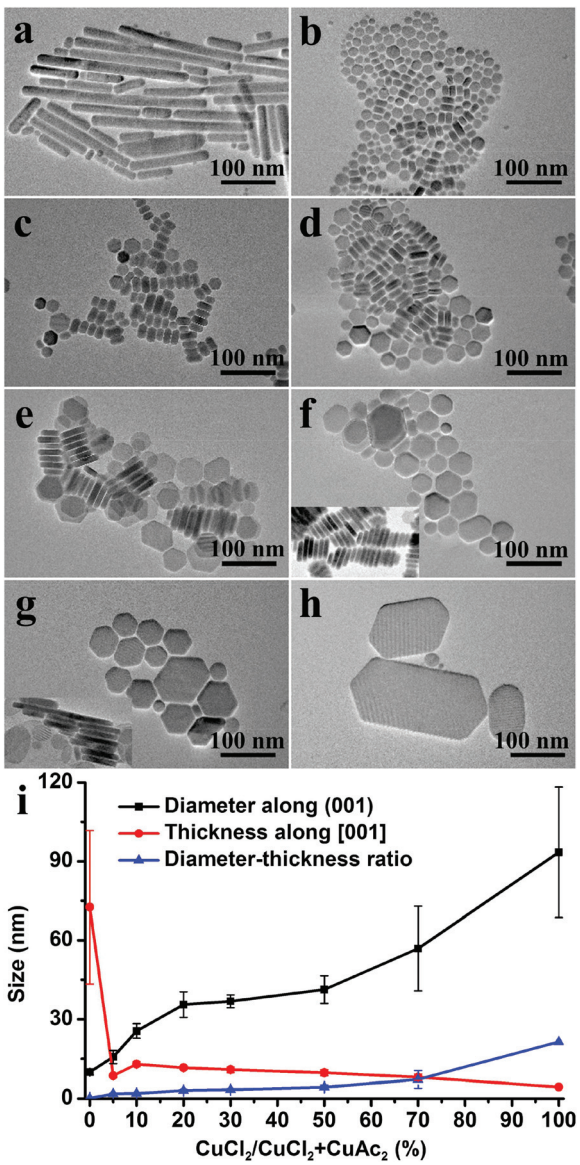

Fig. 6 TEM images of $Cu_{2-x}S$ nanocrystals that are prepared with $CuCl_2$-to-$CuAc_2$ molar feed ratios of 0/10 (a), 0.5/9.5 (b), 1/9 (c), 2/8 (d), 3/7 (e), 5/5 (f), 7/3 (g) and 10/0 (h). The insets in (f) and (g) are the cross section TEM images. (i) $Cu_{2-x}S$ size evolution *versus* $CuCl_2/CuCl_2$ + $CuAc_2$.

4. Conclusions

In summary, we demonstrate the analogous chloride-directed Cu nanocluster self-assembly and the subsequent growth of $Cu_{2-x}S$ nanocrystals. As to self-assembly, the adsorbed Cl^- lowers the dipolar attraction between the neighboring nanoclusters and leads to the redistribution of the DTs on nanoclusters. As a result, the morphology of Cu nanocluster assemblies changes from 1D SANWs to 2D SANRs and SASs with the increase of chloride. The following growth of $Cu_{2-x}S$ nanocrystals is attributed to the fusion of Cu nanoclusters and the reaction with the S from DT decomposition. The Cl^- selectively adsorbs on the (002) facets of $Cu_{2-x}S$ nanocrystals and suppresses the growth along the [002] direction. Consequently, the morphology of $Cu_{2-x}S$ changes from 1D nanorods to 2D nanodisks and nanosheets with the increase of chloride. The analogous Cu nanocluster self-assembly and the growth of $Cu_{2-x}S$ nanocrystals in the presence of chloride give the hope to find new methods for directing nanocluster self-assembly by virtue of the existing approaches to control the morphologies of colloidal nanocrystals.

Acknowledgements

This work was supported by the National key research and development program of China (2016YFB0401701), the NSFC (51425303 and 21404015), the 973 Program of China (2014CB643503), and the Special Project from MOST of China.

References

1 K. S. Novoselov, A. K. Geim, S. V. Morozov, D. Jiang, Y. Zhang, S. V. Dubonos, I. V. Grigorieva and A. A. Firsov, *Science*, 2004, **306**, 666–669.
2 H. Dai, *Acc. Chem. Res.*, 2002, **35**, 1035–1044.
3 Z. W. Pan, Z. R. Dai and Z. L. Wang, *Science*, 2001, **291**, 1947–1949.
4 V. F. Puntes, K. M. Krishnan and A. P. Alivisatos, *Science*, 2001, **291**, 2115–2117.
5 M. H. Huang, S. Mao, H. Feick, H. Yan, Y. Wu, H. Kind, E. Weber, R. Russo and P. Yang, *Science*, 2001, **292**, 1897–1899.
6 R. Jin, Y. C. Cao, E. Hao, G. S. Metraux, G. C. Schatz and C. A. Mirkin, *Nature*, 2003, **425**, 487–490.
7 M. Nasilowski, B. Mahler, E. Lhuillier, S. Ithurria and B. Dubertret, *Chem. Rev.*, 2016, **116**, 10934–10982.
8 C. Tan, X. Cao, X. J. Wu, Q. He, J. Yang, X. Zhang, J. Chen, W. Zhao, S. Han, G. H. Nam, M. Sindoro and H. Zhang, *Chem. Rev.*, 2017, **117**, 6225–6331.
9 Y. Xia, X. Xia and H. C. Peng, *J. Am. Chem. Soc.*, 2015, **137**, 7947–7966.
10 X. Wang and Y. D. Li, *J. Am. Chem. Soc.*, 2002, **124**, 2880–2881.
11 Z. Tang, Z. Zhang, Y. Wang, S. C. Glotzer and N. A. Kotov, *Science*, 2006, **314**, 274–278.
12 Z. Tang, N. A. Kotov and M. Giersig, *Science*, 2002, **297**, 237–240.
13 C. Schliehe, B. H. Juarez, M. Pelletier, S. Jander, D. Greshnykh, M. Nagel, A. Meyer, S. Foerster, A. Kornowski, C. Klinke and H. Weller, *Science*, 2010, **329**, 550–553.
14 S. H. Sun, C. B. Murray, D. Weller, L. Folks and A. Moser, *Science*, 2000, **287**, 1989–1992.
15 Z. Nie, A. Petukhova and E. Kumacheva, *Nat. Nanotechnol.*, 2010, **5**, 15–25.
16 J. W. Liu, H. W. Liang and S. H. Yu, *Chem. Rev.*, 2012, **112**, 4770–4799.
17 H. Y. Fan, K. Yang, D. M. Boye, T. Sigmon, K. J. Malloy, H. F. Xu, G. P. Lopez and C. J. Brinker, *Science*, 2004, **304**, 567–571.
18 T. P. Bigioni, X.-M. Lin, T. T. Nguyen, E. I. Corwin, T. A. Witten and H. M. Jaeger, *Nat. Mater.*, 2006, **5**, 265–270.
19 M. De Graef and M. E. McHenry, *Structure of Materials*, Cambridge University Press, Cambridge, UK, 2012.
20 L. Wang, L. Xu, H. Kuang, C. Xu and N. A. Kotov, *Acc. Chem. Res.*, 2012, **45**, 1916–1926.
21 K. J. M. Bishop, C. E. Wilmer, S. Soh and B. A. Grzybowski, *Small*, 2009, **5**, 1600–1630.
22 K. C. Ng, I. B. Udagedara, I. D. Rukhlenko, Y. Chen, Y. Tang, M. Premaratne and W. Cheng, *ACS Nano*, 2012, **6**, 925–934.
23 X. Peng, L. Manna, W. Yang, J. Wickham, E. Scher, A. Kadavanich and A. P. Alivisatos, *Nature*, 2000, **404**, 59–61.
24 D. Seo, J. C. Park and H. Song, *J. Am. Chem. Soc.*, 2006, **128**, 14863–14870.
25 C. C. Li, W. P. Cai, B. Q. Cao, F. Q. Sun, Y. Li, C. X. Kan and L. D. Zhang, *Adv. Funct. Mater.*, 2006, **16**, 83–90.
26 M. R. Langille, M. L. Personick, J. Zhang and C. A. Mirkin, *J. Am. Chem. Soc.*, 2012, **134**, 14542–14554.
27 P. Liu, R. Qin, G. Fu and N. Zheng, *J. Am. Chem. Soc.*, 2017, **139**, 2122–2131.
28 M. Kruszynska, H. Borchert, A. Bachmatiuk, M. H. Rummeli, B. Buchner, J. Parisi and J. Kolny-Olesiak, *ACS Nano*, 2012, **6**, 5889–5896.
29 M. B. Sigman, A. Ghezelbash, T. Hanrath, A. E. Saunders, F. Lee and B. A. Korgel, *J. Am. Chem. Soc.*, 2003, **125**, 16050–16057.
30 B. Lim, M. Jiang, J. Tao, P. H. C. Camargo, Y. Zhu and Y. Xia, *Adv. Funct. Mater.*, 2009, **19**, 189–200.
31 Z. Wu, J. Liu, Y. Li, Z. Cheng, T. Li, H. Zhang, Z. Lu and B. Yang, *ACS Nano*, 2015, **9**, 6315–6323.
32 Z. N. Wu, Y. C. Li, J. L. Liu, Z. Y. Lu, H. Zhang and B. Yang, *Angew. Chem., Int. Ed.*, 2014, **53**, 12196–12200.
33 L. Li and Q. Wang, *ACS Nano*, 2013, **7**, 3053–3060.
34 X. Jia, J. Li and E. Wang, *Chem. Commun.*, 2014, **50**, 9565–9568.
35 Nonappa, T. Lahtinen, J. S. Haataja, T.-R. Tero, H. Häkkinen and O. Ikkala, *Angew. Chem., Int. Ed.*, 2016, **55**, 16035–16038.

36 R. Jin, C. Zeng, M. Zhou and Y. Chen, *Chem. Rev.*, 2016, **116**, 10346–10413.
37 Y. Negishi, Y. Takasugi, S. Sato, H. Yao, K. Kimura and T. Tsukuda, *J. Am. Chem. Soc.*, 2004, **126**, 6518–6519.
38 R. S. Dhayal, W. E. van Zyl and C. W. Liu, *Acc. Chem. Res.*, 2016, **49**, 86–95.
39 Q. Yao, X. Yuan, Y. Yu, Y. Yu, J. Xie and J. Y. Lee, *J. Am. Chem. Soc.*, 2015, **137**, 2128–2136.
40 W. van der Stam, Q. A. Akkerman, X. Ke, M. A. van Huis, S. Bals and C. D. M. Donega, *Chem. Mater.*, 2015, **27**, 283–291.
41 X. Huang, Y. Li, Y. Li, H. Zhou, X. Duan and Y. Huang, *Nano Lett.*, 2012, **12**, 4265–4270.
42 J. Pérez-Juste, L. M. Liz-Marzán, S. Carnie, D. Y. C. Chan and P. Mulvaney, *Adv. Funct. Mater.*, 2004, **14**, 571–579.
43 A. Rai, A. Singh, A. Ahmad and M. Sastry, *Langmuir*, 2006, **22**, 736–741.
44 M. R. Kim, K. Miszta, M. Povia, R. Brescia, S. Christodoulou, M. Prato, S. Marras and L. Manna, *ACS Nano*, 2012, **6**, 11088–11096.
45 M. Meyns, F. Iacono, C. Palencia, J. Geweke, M. D. Coderch, U. E. A. Fittschen, J. M. Gallego, R. Otero, B. H. Juárez and C. Klinke, *Chem. Mater.*, 2014, **26**, 1813–1821.
46 S. E. Lohse, N. D. Burrows, L. Scarabelli, L. M. Liz-Marzán and C. J. Murphy, *Chem. Mater.*, 2014, **26**, 34–43.
47 Z. Wu, J. Liu, Y. Gao, H. Liu, T. Li, H. Zou, Z. Wang, K. Zhang, Y. Wang, H. Zhang and B. Yang, *J. Am. Chem. Soc.*, 2015, **137**, 12906–12913.
48 M. Ladd and R. Palmer, *Structure determination by X-ray crystallography*, Plenum Press, New York, USA, 2nd edn, 1985.
49 M. J. Turo and J. E. Macdonald, *ACS Nano*, 2014, **8**, 10205–10213.
50 Y. Feng, Q. Yao, J. Li, N. Goswami, J. Xie and J. Yang, *Nano Res.*, 2016, **9**, 942–950.
51 H.-G. Liao, L. Cui, S. Whitelam and H. Zheng, *Science*, 2012, **336**, 1011–1014.
52 T. H. Larsen, M. Sigman, A. Ghezelbash, R. C. Doty and B. A. Korgel, *J. Am. Chem. Soc.*, 2003, **125**, 5638–5639.
53 S.-W. Hsu, W. Bryks and A. R. Tao, *Chem. Mater.*, 2012, **24**, 3765–3771.
54 W. P. Lim, C. T. Wong, S. L. Ang, H. Y. Low and W. S. Chin, *Chem. Mater.*, 2006, **18**, 6170–6177.
55 M. D. Regulacio, C. Ye, S. H. Lim, M. Bosman, L. Polavarapu, W. L. Koh, J. Zhang, Q.-H. Xu and M.-Y. Han, *J. Am. Chem. Soc.*, 2011, **133**, 2052–2055.
56 Y. Xie, A. Riedinger, M. Prato, A. Casu, A. Genovese, P. Guardia, S. Sottini, C. Sangregorio, K. Miszta, S. Ghosh, T. Pellegrino and L. Manna, *J. Am. Chem. Soc.*, 2013, **135**, 17630–17637.
57 S.-W. Hsu, K. On and A. R. Tao, *J. Am. Chem. Soc.*, 2011, **133**, 19072–19075.
58 Y. Zhao, H. Pan, Y. Lou, X. Qiu, J. Zhu and C. Burda, *J. Am. Chem. Soc.*, 2009, **131**, 4253–4261.
59 W. Han, L. Yi, N. Zhao, A. Tang, M. Gao and Z. Tang, *J. Am. Chem. Soc.*, 2008, **130**, 13152–13161.